Design and Fabrication of Low-Loss Toroidal Air-Core Inductors

C. R. Sullivan
S. Prabhakaran
Weidong Li
Shanshan Lu

Found in *IEEE Power Electronics Specialists Conference,* June 2007, pp. 1754–1759.

Design and Fabrication of Low-Loss Toroidal Air-Core Inductors

Charles R. Sullivan, Weidong Li, Satish Prabhakaran and Shanshan Lu
Thayer School of Engineering at Dartmouth, Hanover, NH 03755,
http://power.thayer.dartmouth.edu chrs@dartmouth.edu

***Abstract*— The design and fabrication of high-Q air-core toroidal inductors are described. Designs are optimized for maximum Q for a given size and inductance, independent any particular fabrication process. A fabrication process using a combination of thin-film processes and conventional machining has been used to make prototypes. Measurements performed on the first prototypes confirm the predicted Q of 115 at 50 MHz.**

***Keywords* - inductor, fabrication, optimization, air-core, very-high-frequency (VHF) power conversion**

I. Introduction

Advances in both semiconductor devices and circuit designs are enabling some experimental power conversion circuits to operate efficiently with switching frequencies in the range of 10s of MHz [1], [2], [3], [4]. Most such circuits use resonant circuits for soft switching, impedance matching, and absorbing parasitics. This requires low-loss high-frequency inductors; often several are required for a single power stage. In this frequency range, low-loss magnetic materials are difficult to find, but, because the inductances needed are small, they can be readily achieved using air-core inductors. This is attractive for many reasons: The cost and weight of a core are avoided, and problems with magnetic saturation, nonlinearity, and permeability variation with temperature and time are eliminated [5], [6], [7].

However, skin-effect and proximity-effect losses can make it difficult to design a low-loss inductor at these frequencies. In addition, most air-core inductors have a large external field, which can cause electromagnetic interference (EMI) and electromagnetic compatibility (EMC) problems. And nearby conductors or semiconductors, often including the substrate on which the inductor is formed, can have eddy currents induced in them, incurring losses and causing variation of the inductance.

A toroidal configuration solves many of these problems [8]. Wire-wound toroids are widely used and readily available, but the wire winding process is expensive and results in a sub-optimal configuration. Improved toroidal inductors have been constructed by microfabrication [8] or by wire winding with specially shaped wire [9]. This paper describes optimization, fabrication, and testing of toroidal inductors that better approach the ideal best possible performance for a given size.

Section II describes the designs which are optimized independent of the limitations of any particular fabrication process. The performance metric used is quality factor Q rather than power handling or power loss because of the linearity of air-core inductors. An effective Q also considering the effect of dc resistance [10] is also considered. The design optimization results are useful not only for achieving the maximum possible performance with toroidal air-core inductors, but also for providing information on what is achievable, information that is essential for use in designing circuits and systems that use the such inductors.

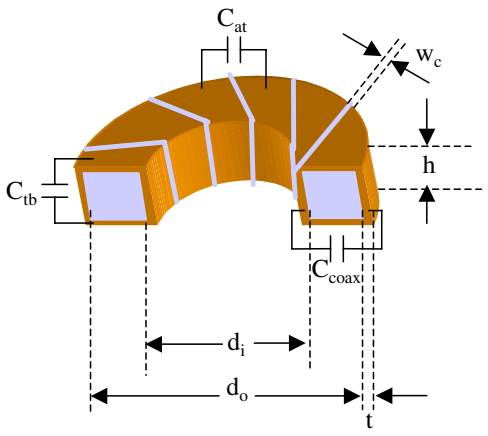

Fig. 1. Schematic of the cross-section of a toroidal air-core inductor. Dimensions and capacitances associated with the device are also included.

In Section III, a fabrication process using a combination of thin-film processes and conventional machining is used to make prototypes which closely approximate the ideal. Measurements (Section IV) confirm predicted Q performance.

II. Design of Air-Core Toroidal Inductors

At high frequency, skin effect constrains current to flow only on the inside surface of a toroidal winding, facing the interior high-field region. Achieving the minimum ac resistance for a given size and number of turns requires making maximal use of that surface. A flat conductor surface, for example as achieved in [8], will have less current crowding than the ridged surface of a wire-wound toroid [11], [12], [13]. Thus, we consider designs similar to those in [8], with a foil-like conductor conforming to the shape of the toroid, which we fabricate as shown Fig. 6 and discussed in Section III. In this section we discuss the design process for maximizing Q in such an inductor.

Fig. 1 is a schematic of the cross-section of an air-core toroid. A rectangular cross-section was initially chosen for convenience in fabrication, and because it provides a larger flux path in a given volume than the circular cross section

used in [8]. Other possible cross sections are discussed in Section II-A.

The rectangular cross-section geometry is described by the inner diameter d_i, outer diameter d_o, height h, conductor thickness t, slit width w_c between adjacent turns, and number of turns N. The inductance of the structure may be calculated as the sum of the inductance due to the field inside the toroid [14] plus the inductance of a single-turn loop around the center hole of the toroid:

$$L = \frac{N^2 h \mu_0}{2\pi} \ln\left(\frac{d_o}{d_i}\right) + \frac{d_i + d_o}{4}\mu_0 \left[\ln\left(8\frac{d_o + d_i}{d_o - d_i}\right) - 2\right] \quad (1)$$

where μ_0 is the permeability of free space.

Ac current flows in a skin-depth on the inner surface of the winding. Stray magnetic field in the region containing the slits lead to current crowding at the edges of windings that face the slits and affects the ac resistance, as shown in the finite-element simulation in Fig. 2. To account for this effect, we first considered a hypothetical single-turn design, and calculated the ac conductance, G_0. We postulated that the conductance decreases for each slit that is added. Hence for N slits,

$$G_{single-turn} = \frac{1}{R_{single-turn}} = G_0 - N \cdot G_{slit} \quad (2)$$

where $G_{single-turn}$ is the ac conductance of a single turn with N slits and $R_{single-turn}$ is the corresponding ac resistance. For an N-turn design (with N slits), the total ac resistance R_{ac} is calculated as

$$R_{ac} = N^2 R_{single-turn} = \frac{N^2}{G_0 - N \cdot G_{slit}} \quad (3)$$

A model for G_{slit} was determined as a function of slit width by curve fitting to results of finite element analysis.

$$G_{slit} = (0.515 w_c - 1\,\mu\text{m})\delta \ell_t \quad (4)$$

where w_c is the width of the slit cut between turns, δ is the electromagnetic skin depth, and ℓ_t is the length of a turn (twice the height plus the difference between inside and outside diameter).

The model does not capture the effect of curvature (determined by d_o or d_i), interaction between slits (determined by the spacing between them), or conductor thickness t. The model is based on simulations of slit widths w_c up to 150 μm at 50 MHz. Our optimization results indicate that optimized designs fall within the range analyzed, and so our model is useful in this range. Note that the incremental decrease in conductance due to the slit is less than a simple model, based only on subtracting a fraction of the surface, would predict. This is because, as can been seen in Fig. 2, some current flows on the inside edges of the slit, in addition to flowing on the main surface of the conductor.

Fig. 1 also shows the various capacitances in the device. We consider three regions that contribute the most significant capacitance; the capacitance formed across a slit between

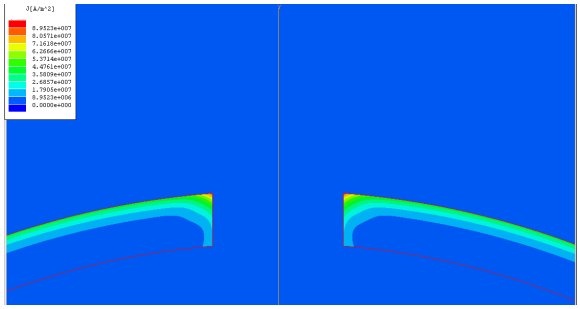

Fig. 2. Current density (indicated by shading) calculated by finite-element analysis near the slit between two turns on the inside perimeter of a toroidal inductor. Current flows along the surface facing the interior high-field region; slight current crowding is apparent at the corners.

adjacent turns C_{at}, the capacitance formed between the top and bottom of horizontal sections of a single turn C_{tb}, and the capacitance formed between the inner and outer vertical sections of a single turn C_{coax} (Fig. 1). C_{at} includes the sum of the parallel plate capacitance inside the slit and the fringing capacitances in the dielectric on the inside of the toroid and that in the air on the outside. The calculation of the fringing capacitance was performed by determining a fringing coefficient based on w_c, t and d_o as developed in [15] for magnetic fields in the same geometry. C_{coax} and C_{tb} are derived from standard formulas for capacitance for a coaxial configuration and a parallel plate configuration, respectively.

The effective total capacitance between the terminals of the inductor C includes the series and parallel combinations these capacitances. For example, consider the effective total capacitance due to the the turn-to-turn capacitances C_{at}. This includes a series string of $N-1$ capacitors of value C_{at}, in parallel with with a single capacitor also of value C_{at} between the first and last turns. A similar calculation is used for C_{coax} and C_{tb}. The total capacitance (C) is the sum of the effective contributions due to C_{at}, C_{coax} and C_{tb}. The equivalent circuit for the inductor is then modelled as a series LR_{ac} circuit in parallel with C in order to calculate Q.

For a given inductance specification L at a given frequency f (e.g., 50 MHz) and with a size constraint placed on d_o (20 mm) and h (5 mm), the design goal was to find the combination of d_i, w_c and N that would exhibit the maximum Q. The remaining parameters have conflicting requirements with respect to maximizing Q. For example, a large w_c favors lower capacitance but results in higher R_{ac}. Hence the choice of these parameters was achieved through an optimization process that maximized Q by assessing such tradeoffs. For a given L, f, d_o, h a numerical optimization (the Nelder-Mead simplex algorithm as implemented in MATLAB [16]) was used to determine designs with maximized Q. Fig. 3 shows the calculated Q of the optimized designs for a range of inductances for $d_o = 20$ mm and $h = 5$ mm at 50 MHz with a copper conductor at room temperature.

Fig. 4 shows the calculated Q of the optimized designs over a range of frequencies for several sizes. Since smaller

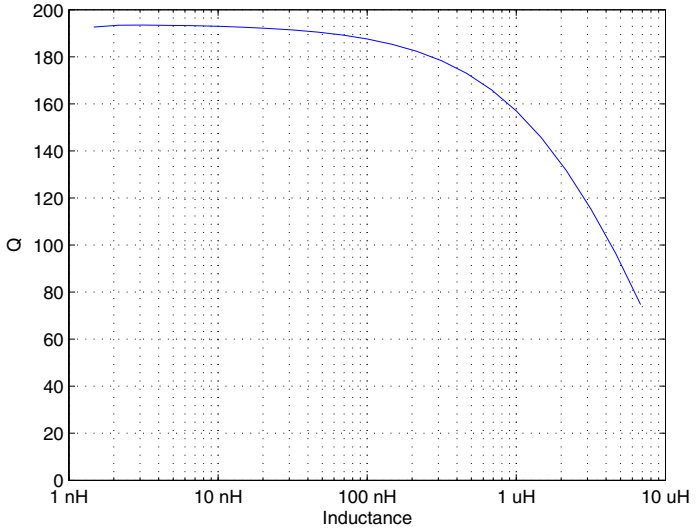

Fig. 3. Q of the optimized designs for a range of inductances for $d_o = 20$ mm and $h = 5$ mm at 50 MHz.

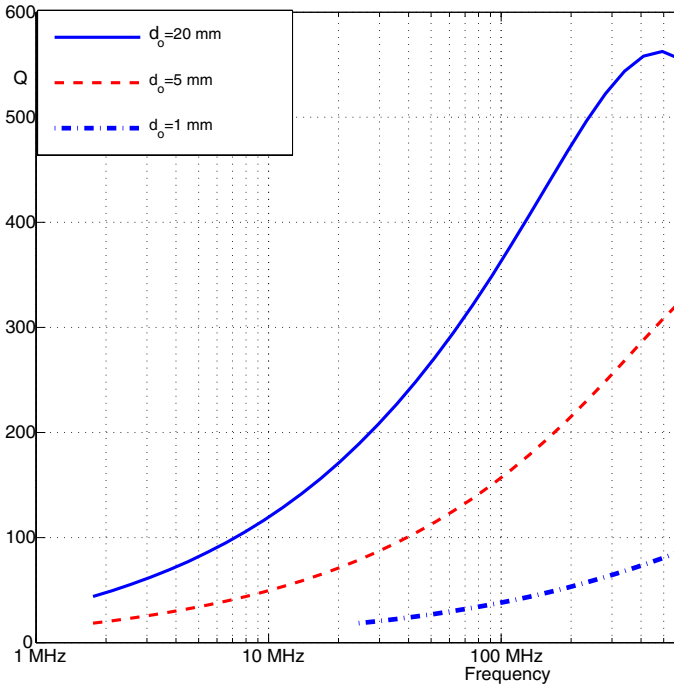

Fig. 4. Q of the optimized designs over a range of frequencies for several diameters, all for $h = 5$ mm and 50 Ω inductive reactance.

inductance values are typically needed at higher frequencies, this plot is based on an inductive impedance of magnitude 50 Ω rather than a single inductance value for the whole frequency range.

A. Shape Optimization

Although the overall optimization assumes a rectangular cross section for the toroid, this is not necessarily the optimum shape. Optimal shapes of low-frequency air-core toroidal inductors are addressed thoroughly in [12]. However these shapes do not apply here directly because of the skin effect

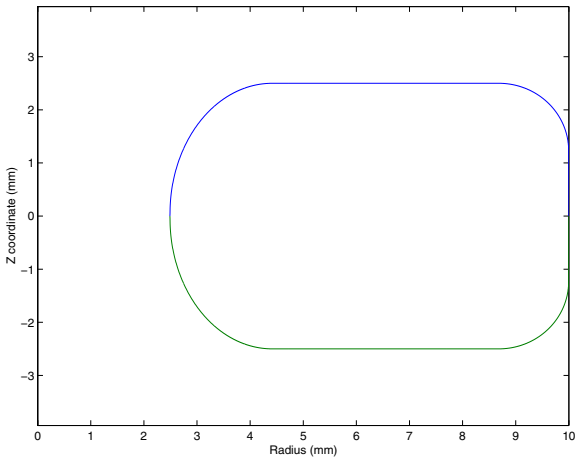

Fig. 5. Optimized cross section shape.

and because we are applying a height constraint. To investigate the potential improvement from other shapes, we numerically optimized cross-sectional shapes based on maximizing Q considering only the ac resistance and the inductance, assuming that the shape would not have an important effect on capacitance.

The first optimization used as independent variables the inner radius and the z coordinates of a set of points equally spaced from the inner radius to the outer radius. The optimization did not consistently converge to a clear global minimum. However, the convergence was sufficient to show the general characteristics of the best shapes: close to a rectangle but with rounded corners, more rounded at the inside and closer to square at the outside. An improvement in Q of 6.6% over the rectangular cross section was obtained for 20 mm diameter with height of 5 mm.

In order to make the optimization problem more tractable, a less general set of shapes with rounded corners, described by fewer parameters, was used next: elliptical corners parameterized by the major and minor axes of the ellipse. With the inner radius, the total number of parameters is five. The Q was optimized numerically, using the same numerical evaluation of resistance and inductance used for the unconstrained optimization. This improved the convergence of the optimization, and led to the shape shown in Fig. 5, which provides an 8.3% improvement over the rectangular cross section.

In practice, we used a rectangular cross section for ease of fabrication, knowing that we gave up less than 10% in Q compared to an optimized cross section.

B. Performance Evaluation and Comparison

A conventional wire-wound solenoidal air-core RF inductor can achieve slightly higher Q in the same volume compared to the inductors considered here, if only the volume of the component itself is considered. However, such an inductor requires a large space free of conductors in order to avoid having the Q degraded or the inductance value disturbed: the main advantage of the present designs compared to a solenoid is the nearly complete absence of an external field. The conventional solution that comes closes to approximating that advantage is a wire-wound air-core toroid. Compared to a wire-wound air-core toroid, the present designs offer three advantages:

- The external field is much smaller than the external field of a wire-wound toroid, which can be significant near the outer wires, which are spaced further apart than the inside diameter. This effect is most severe for smaller numbers of turns.
- The capacitance between turns is smaller because of the plated copper can be thin compared to round wires.
- The ac resistance is lower because of the smooth copper surface facing the high-field interior of the inductor, which avoids the current crowding effects in a wire winding.

To quantitatively asses this last effect for one representative example, a two-dimensional finite-element simulation of an 8-turn wire-wound toroid was compared to a simulation of one of our designs, using the same diameter and height. Q was calculated considering only ac resistance and inductance, ignoring capacitive effects. The Q value for our design was 60% higher than that of the wire-wound component.

At frequencies in the range of tens of MHz, resonant circuit designs are almost always used. In such circuits, most inductors are required to handle current waveforms with large ac components, often larger than the dc component. In this case, the dc loss is often negligible; hence our design approach based on ac only. However, in some applications, dc resistance may be more important. For these cases, we note that the dc resistance of our designs is typically much lower than the ac resistance. For example, at 50 MHz, the skin depth is 10 μm; if the copper is 50 μm thick, the dc resistance is one fifth the ac resistance. For typical PWM applications, an effective Q equal to

$$Q_{eff} = \frac{\omega L}{\frac{1}{4}R_{ac} + \frac{3}{4}R_{dc}} \tag{5}$$

has been proposed [10]. In the case of 50 MHz operation with copper 50 μm thick, the result is a Q_{eff} 2.5 times higher than Q. This shows that relatively small, low-Q designs would be adequate for situations in which ac loss is relatively unimportant.

III. Fabrication

The initial prototypes were fabricated using a combination of conventional machining and thin-film deposition processes in order to allow rapid development of prototypes; various variations on the process are under consideration to make larger-scale manufacturing more cost-effective and to achieve higher-resolution patterning. The first set of prototypes was fabricated using a polycarbonate substrate machined in a toroidal shape, 10 mm in diameter and 2 mm thick. A thin copper seed layer (about 1 μm-thick) was deposited on all surfaces of the substrate by performing several sputter

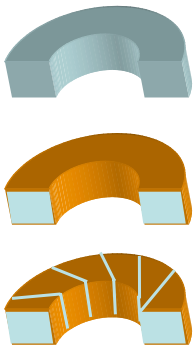

Fig. 6. Steps involved in the fabrication process.

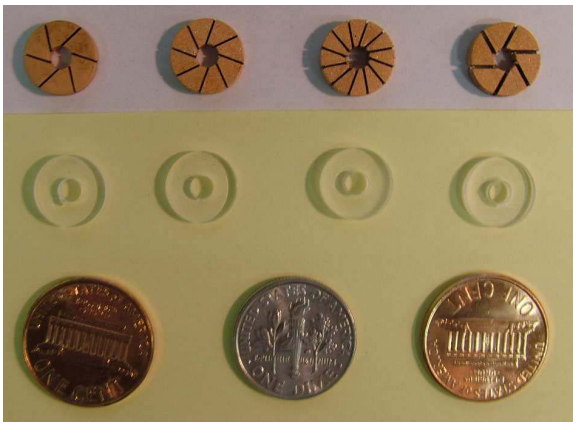

Fig. 7. Fabricated inductors: 6, 8, and 12 turns; 0.25 mm and 0.5 mm slit widths.

depositions. The copper thickness was then supplemented by electroplating additional copper for a total thickness of approximately 50 μm, more than is necessary for the 10-μm skin depth in copper at 50 MHz. The steps described above effectively completed an inductor with one shorted turn. The copper was then cut to make multiple turns, using conventional machining with a 0.010" (0.254 mm) end mill, leaving a 0.010" space between the turns. These steps are shown in Fig. 6. Fig. 7 is a photograph of four different inductors we have fabricated.

The initial prototypes were designed for several tens of nH at 50 MHz. For higher inductance with the same physical size, more turns are needed and finer spacings between turns (25 μm–100 μm) are desirable to maintain low resistance. We have tested two methods of cutting finer slits between turns after using the same sputtering and electroplating process to deposit the copper. The first was similar in concept to photolithography, in that we coated the copper to protect it from etchant, and opened slits in this resist coating to allow corresponding slits to be etched in the copper. However, because photolithography would be difficult on the three-dimensional surface, particularly in the interior surfaces of the hole, we instead slit the resist coating with a scalpel blade, held fixed while the inductor was moved with optical micro-

Fig. 8. Slits cut between turns by sawing, as discussed in the text. The diameter of the center hole shown in 4 mm.

TABLE I

INDUCTOR PERFORMANCE

	Inductance	Q at 50 MHz	ESR at 50 MHz
Calculation	16 nH	132	45 mΩ
Direct measurement	19 nH	144*	41 mΩ*
Indirect measurement**	Not needed	115	52 mΩ

*Not expected to be accurate

** Q based on scaling measured 10 MHz ESR (23.2 mΩ) up by the square root of 5

positioning equipment. After testing several resist materials, we found that shellac performed best for this process. Although we demonstrated clean slits about 50 μm in width on flat substrates, achieving the necessary uniform coating of shellac on three-dimensional toroids proved more difficult. Although we successfully used this process to make the coil on the magnetic-core inductor reported in [17], the final slit widths were poorly controlled.

To more cleanly and reliably form small slits, we developed a sawing process, using a small circular saw blade for most surfaces and a scroll saw for slits in the interior hole. Typical saw blades have the individual teeth splayed outwards (*set*) in order to cut a kerf slightly wider than the thickness of the blade itself, thus avoiding binding. However, the depth of the cuts we need to make is only about 50 μm, much less than the depth of the teeth themselves. Thus, no set is needed, and in fact the teeth can be thinned near the tips to allow cutting a slit thinner than the main body of the blade. Such blades were made by grinding the teeth of conventional saw blades to remove the set and narrow the tips of the teeth, similarly to sharpening a knife blade. The inductor was positioned on a scroll saw using optical micro-positioning equipment for the interior cuts; for exterior cuts, the small circular saw blade was used with a milling machine. Our initial tests of this method have produced clean cuts about 100 μm wide, as shown in Fig. 8. We expect that thinner cuts would be possible, although that becomes important only for large numbers of turns.

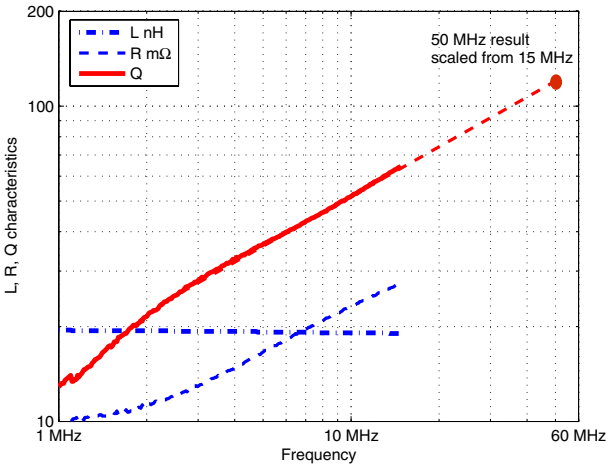

Fig. 9. Plot of measured inductance, ESR, and Q as a function of frequency, including projections to higher frequencies than those measured.

IV. Measured Results

A precision impedance analyzer (Agilent 4294A) was used to measure the inductance and Q of the 6-turn inductor with 0.25 mm slit width. A low-residual-inductance test fixture [18] was used to connect the inductor. Since Q of the inductor is high, the ESR is very small compared to the imaginary part of the impedance. Thus even small phase error may result in a large measurement error. For example, measuring a Q of 100 with 10% accuracy requires a phase accuracy of 0.05 degrees. The impedance analyzer switches modes at 15 MHz, and only gives sufficient phase accuracy below 15 MHz. Thus, we do not have a valid direct measurement of Q at our design frequency of 50 MHz. In the frequency range of interest, Q is proportional to the square root of frequency, because loss is dominated by simple skin-effect resistance (which is inversely proportional to the square root of frequency). Results below 15 MHz confirm this scaling trend very well, as shown in Fig. 9. Thus, at present, our best experimental assessment of Q at 50 MHz comes from 10 MHz measurements, scaled for the frequency difference. Comparing either the 10 MHz measurement or the 50 MHz result derived from the 10 MHz measurement shows that the loss is 15% higher than the loss calculated by the methods discussed in Section II. Note that the slits in the measured prototype were wider than the optimum slit widths would be. Thus, we have not directly confirmed the performance of designs chosen according to the optimization process.

V. Conclusion

Air-core toroidal inductors have been fabricated using a combination of thin-film processes and conventional machining. Measurements performed on the first prototypes confirm the predicted Q of 115 at 50 MHz. Optimizations aimed at maximizing Q of a given geometry and impedance have been presented. The optimization process can be implemented independent of the limits of any particular fabrication process. It shows that inductors with Q over 200 are possible from 30 MHz to 2 GHz.

References

[1] J. M. Rivas, D. Jackson, O. Leitermann, A. D. Sagneri, Y. Han, and D. J. Perreault, "Design considerations for very high frequency dc-dc converters," in *37th IEEE Power Electronics Specialists Conference*, 2006.

[2] T. Suetsugu and M. K. Kazimierczuk, "Integrated class DE synchronized dc-dc converter for on-chip power supplies," in *37th IEEE Power Electronics Specialists Conference*, 2006.

[3] J. M. Rivas, Y. Han, O. Leitermann, A. Sagneri, and D. Perreault, "A high-frequency resonant inverter topology with low voltage stress," in *38th IEEE Power Electronics Specialists Conference*, 2007.

[4] R. Pilawa-Podgurski, A. Sagneri, J. Rivas, D. Anderson, and D. Perreault, "Very high frequency resonant boost converters," in *38th IEEE Power Electronics Specialists Conference*, 2007.

[5] S. Tang, S. Y. Hui, and H.-H. Chung, "Coreless planar printed-circuit-board (PCB) transformers—a fundamental concept for signal and energy transfer," *IEEE Trans. on Power Electronics*, vol. 15, no. 4, pp. 931–941, 2000.

[6] ——, "Some electromagnetic aspects of coreless PCB transformers," *IEEE Trans. on Power Electronics*, vol. 15, no. 5, pp. 805–810, 2000.

[7] ——, "Characterization of coreless printed circuit board (PCB) transformers," *IEEE Trans. on Power Electronics*, vol. 15, no. 6, pp. 1275–1282, 2000.

[8] J. Phinney, J. Lang, and D. Perreault, "Multi-resonant microfabricated inductors and transformers," in *35th IEEE Annual Power Electronics Specialists Conference.*, vol. 6, 2004, pp. 4527 – 4536.

[9] Mark Seitz and Michael Roeber, "Squeeze more performance out of toroidal inductors," *Power Electronics Technology Magazine*, pp. 302–33, aug 2005.

[10] E. Waffenschmidt, B. Ackermann, and M. Wille, "Integrated ultra thin flexible inductors for low power converters," in *IEEE Power Electronics Specialists Conference*, 2005.

[11] R. A. M. Browne, S. W. H. D. Haan, J. B. Klaassens, J. D. Lodder, and D. J. Verheul, "Computer-aided design of toroidal air-core inductors for high energy levels," *IEEE Trans. on Industrial Electronics*, vol. 35, no. 2, pp. 329–337, 1988.

[12] P. Murgatroyd, "The optimal form of coreless inductors," *IEEE Transactions on Magnetics*, vol. 25, no. 3, pp. 2670–2677, 1989.

[13] V. Ermolov, T. Lindstrom, H.Nieminen, M. Olsson, M. Read, T. Ryhanen, S. Silanto, and S. Uhrberg, "Microreplicated RF Toroidal Inductor," *IEEE Transactions on Microwave Theory and Techniques*, vol. 52, no. 1, pp. 29–37, 2004.

[14] S. Ramo, J. Whinnery, and T. V. Duzer, *Fields and Waves in Communication Electronics 3rd Ed.* John Wiley and Sons, INC., 1994.

[15] V. Bossche, V. Valchev, and T.Filchev, "Improved approximation for fringing permeances in gapped inductors," in *IEEE Industry Applications Society 2002*, vol. 2, 2002, pp. 932–938.

[16] J. Lagarias, J. Reeds, M. Wright, and P. Wright, "Convergence properties of the Nelder-Mead simplex method in low dimensions," *SIAM Journal on Optimization*, vol. 9, no. 1, pp. 112–47, 1998.

[17] S. Lu, Y. Sun, M. Goldbeck, D. R. Zimmanck, and C. R. Sullivan, "30-mhz power inductor using nano-granular magnetic material," in *IEEE Power Electronics Specialists Conference*, 2006.

[18] S. Prabhakaran and C. R. Sullivan, "Impedance-Analyzer Measurements of High Frequency Power Passives: Techniques for High Power and Low Impedance," in *IEEE Industry Applications Society Annual Meeting*, Oct. 2002.